7C.4 CREATING DIAGNOSTIC TECHNIQUES OF TC STRUCTURE FROM SATELLITE MICROWAVE DATA TOWARD IMPROVED INTENSITY PREDICTION

Joshua Cossuth and Robert E. Hart
Florida State University, Tallahassee, Florida

1. INTRODUCTION

For over two decades, the average error in tropical cyclone (TC) intensity forecasts has remained statistically unchanged (Cangialosi and Franklin 2012). Recent top-performing intensity guidance includes consensus (e.g. Sampson et al. 2008) and statistical (e.g. SHIPS; DeMaria et al. 2005) models. However, despite the fact that TC intensity forecasts are improved by increased observations of structural features inside and around TCs (Burpee et al. 1996), current TC intensity prediction models do not sufficiently incorporate attributes of TC structure.

Using a climatology of operational aircraft reconnaissance vortex messages, Piech (2007) demonstrated specific regimes of inner-core measurements that correspond to a TC's intensity. Murray (2009) has further shown that such observations are skillful at predicting TC intensity. Unfortunately, aircraft data have spatial and temporal limitations that limit their use in operational intensity forecasting.

To contrast, satellite coverage of TCs occurs via multiple platforms with regular, predictable intervals. Common methods to diagnose intensity by satellite, such as the subjective Dvorak technique (e.g. Dvorak 1975) and the objective Advanced Dvorak Technique (ADT; Olander and Velden 2007), implicitly account for complex aspects of TC structure. Though these interrogation schemes provide extremely useful diagnosis of the current TC intensity, they do not provide an account of the variety of TC structures and how those structures relate to future TC intensities.

Not only are the physical processes that govern changes in TC structure poorly defined, but the range and types of structural characteristics have not been fully explored (Wang and Wu 2004). The lack of such a long-term record in TC structure stems from a need to create metrics that identify structural features. The following research describes preliminary steps towards creating objective techniques that quantify a TC's structure, as diagnosed by satellite observations.

2. METHODOLOGY

To perform a broad analysis of TC structural representation, the HURSAT dataset (Knapp 2008) provides a global TC-centered satellite data archive from various platforms. In particular, this analysis will focus on Special Sensor Microwave/Imager (SSM/I) data from the Defense Meteorological Satellite Program (DMSP) series satellites (through HURSAT-MW). These frequencies detect convective hydrometeor signals that are obscured by cirrus canopies in conventional visible and infrared bands, allowing an improved ability to diagnose TC structure (Hawkins et al. 2001).

HURSAT provides position estimates through interpolating the 6-hourly best track positions. Because the best track does not intend to preserve small scale motions, such interpolated positions may not represent the TC's actual location on satellite. Thus, ARCHER analysis software (Wimmers and Velden 2010) is used to analyze a TC center using the satellite data itself.

From the ARCHER-positioned centers, each HURSAT image is transformed into storm-relative polar coordinates. These new images are used to more easily examine storm-by-storm variability between cases. Size and symmetry criteria of TC features, such as the eye and eyewall, are created based on empirical investigations in polar coordinates.

3. OBJECTIVELY CHARACTERIZING THE EYE

Before delving into the results, this section will briefly discuss the importance and implications of correctly (or incorrectly) centering the TC.

While the TC's location is intrinsically valuable and implicitly necessary for track and intensity forecasts, a precisely defined center must be ascertained to perform an analysis of structure. When examining a single storm in polar coordinates, errors in the center position lead to distortions of size and shape in structural features as well as incorrect distance and directional relationships. Such false readings will propagate into compositing schemes and can create erroneous signals.

Polar coordinate transformation of TCs offers an advantage, in that it can be used to both diagnose miscentering and define eye shape asymmetry. Figure 1 provides diagrams for three sample eye representation cases. The top example (a) demonstrates a circular eye with a 'correct' center position in the middle of the circle. This is represented in polar coordinates as a straight line; that is, the eye size is one constant radius for every angle. When the center fix for a circular eye is displaced to the north though (b), a wavenumber 1 asymmetry is found in polar coordinates. Azimuthal averages and feature measurements throughout the image would be off compared to the case (a).

Corresponding author address: Joshua Cossuth, Florida State University, 404 Love Building, Tallahassee, FL 32306-4520; email: jhc06@my.fsu.edu

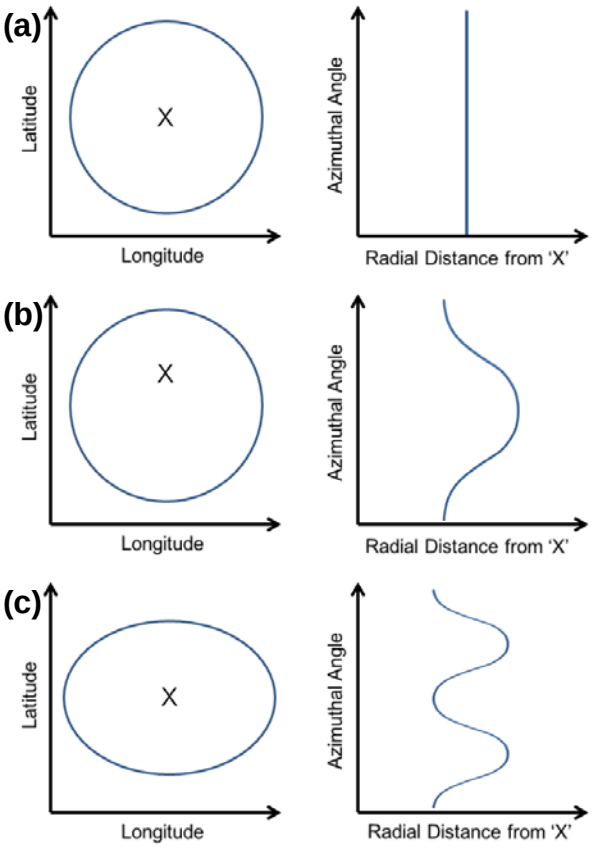

Figure 1. Schematic idealized examples of eye size representations in X-Y coordinates (left) and polar coordinates (right). The center is marked by an 'X' on the left and is represented by the ordinate axis on the right, where 0^o (north) begins at the origin and moves clockwise (up). Top (a): Circular eye with ''correct' center location. Middle (b): Circular eye with center location displaced to the north. Bottom (c): Elliptical eye with the minor (short) semi-axis lying along a meridian.

A correction can be applied to the middle case of Figure 1 to approach the correct center. By summing up the radius at two arbitrary opposing angles (180^o apart), dividing by two, and applying that distance inward from the eye edge, an improved center estimate is obtained. While different angle pairs may yield varied distances, several iterations will converge toward a more precise position.

However, as the bottom of Figure 1 demonstrates, having different eye diameter estimates from various opposing angle pairs can represent eye asymmetry as well. In this case of an elliptical eye with a proper center position (c), the smallest eye diameter (0-180^o) represents the minor semi-axis and the largest eye diameter (90-270^o) represents the major semi-axis.

In addition to objectively estimating the eye and eyewall position, size, and shape in this manner, the percentage of eye and eyewall completion can be similarly found using thresholds of satellite-observed Brightness Temperature (T_B) along a radial path.

4. INTERPRETING A CASE STUDY

An SSM/I overpass of Hurricane Katrina (2005) near peak intensity (Figure 2) is examined as an example case to demonstrate the methods used to objectively quantify structural features of TCs.

There are several notable features in Figure 2. Firstly, there are two marked centers (see inset): the ARCHER derived position ('O'; used in all further analysis) and the interpolated best track ('X'). In this case, the difference between these two estimates is minimized due to clarity of the eye scene and proximity to synoptic time. Concentric radial circles (white inside black lines) are marked by the distance (km) from the ARCHER center. Structurally, this case shows a well-defined eye and inner-core ring, evidence of secondary eyewall formation near 100km, and several banding features, with the majority of the TC's 85GHz signature confined to within 300km of the center. Also note, the absence of shaded T_B values in the lower right is due to the limited swath width of the polar-orbiting satellite.

The top portion of Figure 3 transforms Figure 2 observations into polar coordinates. Features noted above in Figure 2 also appear in Figure 3, but now in relation to distance and direction from the TC center. In particular, the profile of the eye and eye-wall are much easier to discern in Figure 3's polar coordinates and can be compared to the schematics in Figure 1. Depending on the threshold criteria of T_B (shaded), both wavenumbers 1 and 2 can be found near the radius of the boundary between eye and eyewall.

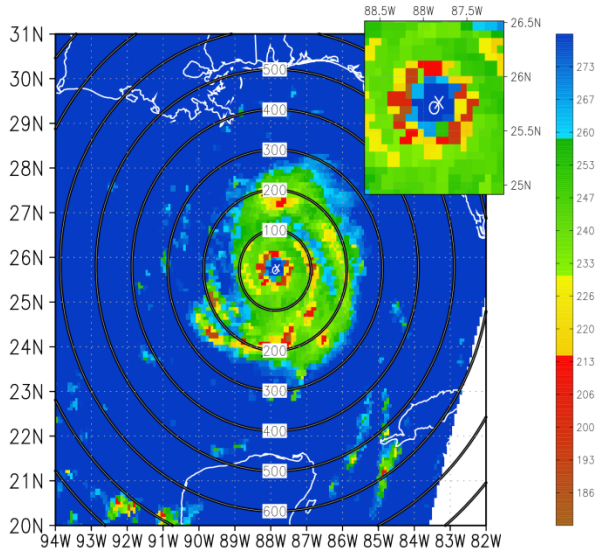

Figure 2. 85GHz polarization corrected temperature of Hurricane Katrina on August 28, 2005, 1244z. Retrieved from HURSAT and measured by the DMSP-F13 SSM/I.

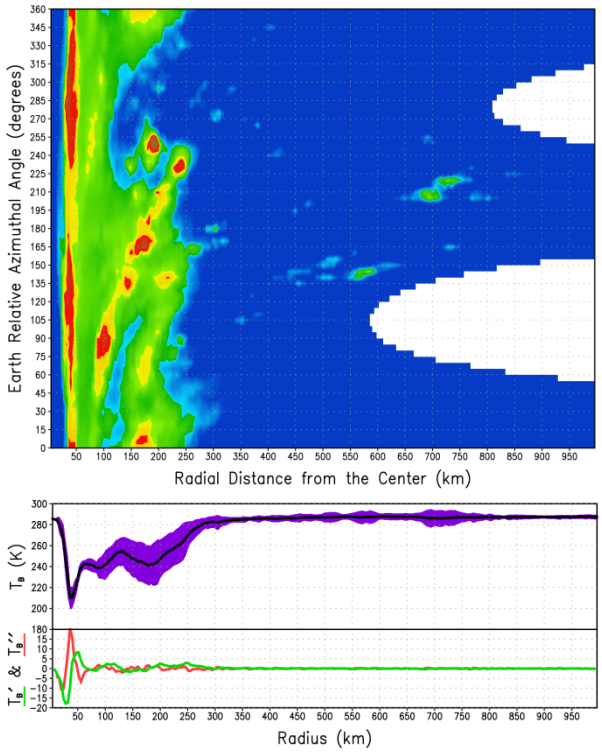

Figure 3. Top: Same as Figure 2 (including color bar), except in storm-relative polar coordinates. The abscissa is the radius outward from the center of the storm (diagnosed by ARCHER); the ordinate is the azimuth (e.g. 180 degrees is south). Middle: Line graph depicting the azimuthal average brightness temperature (T_B) of the top figure, with the standard deviation shaded about the line (in purple). Bottom: The first (green) and second (red) derivatives of the azimuthal average T_B.

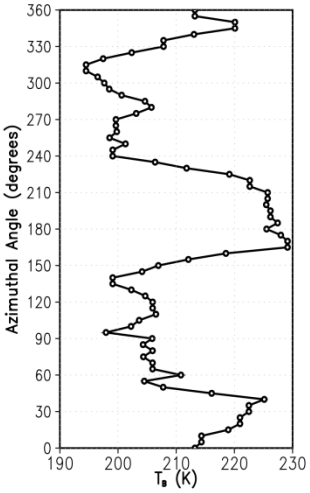

Figure 4 (opposite column; top). Azimuthal profile of T_B at the radius of global average minimum from Figure 3 (valid at 40km from the center).

The middle and bottom panels of Figure 3 show efforts to reduce dependence on particular values of T_B when determining eye size and shape. While these T_B values are important and should be considered in structural analysis, creating structural metrics that do not rely on the precise T_B will help reduce error due to inter-sensor calibration. For example, a threshold criterion of 260K will produce an eye size of 24km (Figure 3 middle panel). Choosing the inflection point between the eye (high T_B) and eyewall (low T_B), where:

Inflection Point (High → Low T_B) = Min($\frac{\partial T_B}{\partial r}$; green line)

supports a 28km radius, while the change in concavity

Concave Up → Down = Min($\frac{\partial^2 T_B}{\partial r^2}$; red line)

suggests an eye radius of 20-24km.

Relying upon cues of shape for TC structure is also advantageous for analysis of TCs that do not correspond to the classic picture of a hurricane. In cases of tropical storms or minor hurricanes without a pronounced eye signature, deepening of convective features can be seen by steeper gradients and sharper derivatives. Likewise, hurricanes eyes smaller than the satellite resolution (e.g. peak intensity Wilma, 2005) can still be inferred by inner-eyewall analysis.

The inner-eyewall of Figure 3 exists near the radius of minimum T_B (40km from the center). A closer examination of the values at that radius reveals several features. Figure 4 shows a wavenumber 2 structure in the T_B values at this radius. This feature primarily relates to inner-core strength at different azimuths, but is also influenced by the eye asymmetry, which extends further outward where the eyewall is weaker.

A simple azimuthal average (as in the middle plot of Figure 3) may be insufficient for identifying spiral or asymmetric features, though the greater standard deviation at the outer storm radii indicate the presence of varied structures. Many linear and discrete structures make up the TC outside of the radius of the inner eyewall. Notably, several banding features that spiral away from the center converge near the 80km radius, which forms the secondary azimuthal average minimum. Likewise, moating features are seen spiral in toward the 60km radius local maximum. Such T_B patterns may indicate future eyewall replacement cycles.

5. COMPOSITING STRUCTURAL FEATURES

After various features of TC structure are objectively identified, comparisons can be made between systems. Composites of TCs with similar characteristics are created to distinguish how different structures are related to each other and intensity.

Figure 5 compares a TC's global minimum azimuthal T_B (on the ordinate) and intensity (abscissa) with the average radius where the minimum azimuthal T_B occurs (in km; shaded). This radius represents where the maximum convection is found in TCs with an eye that is smaller than the sensor resolution or TCs without an eye. For TCs that have a medium-sized eye or larger, this radius is usually associated with middle of the inner-eyewall, as shown in Section 4.

In general, Figure 5 shows that smaller eyewall radii are found to be in more intense TCs and have lower average T_B. The former fact is consistent with conservation of angular momentum. The latter is likely due to a greater number of pixels that compose larger

radii, making it more likely for weaker, non-convective signals (which have higher a T_B signature in 85GHz) to influence the azimuthal average. For weaker systems, an eye is likely not present. In these cases, very small radii and low brightness temperatures represent intense convection near or over the TC center.

However, Figure 5 can also be interpreted beyond TC cases with well-defined inner-cores. The radius maximum near 100 kts and high average T_B (~270 K) may be related to various weakening phases in the TC lifecycle, such as eye-wall replacement cycles (ERCs) found in previous work (e.g. Piech 2007), less favorable environments, or extratropical transition. Asymmetries in convective features may make it likelier for high T_B to influence azimuthal average. Further, a significant presence of non-convective features may contribute to inhibiting further intensification.

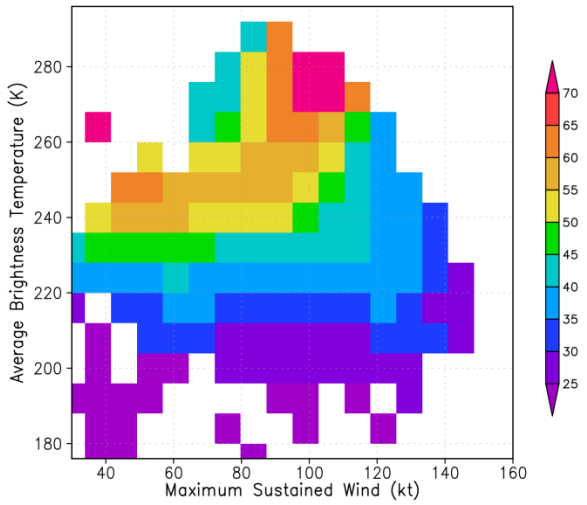

Figure 5. Average radius (in km) of minimum azimuthal T_B, based on the TC intensity (abscissa) and average T_B at that radius. Smoothed once by nine-point averaging. Based on global HURSAT-MW cases that meet ARCHER criteria for center relocation.

6. CONCLUDING DISCUSSION

The techniques and analysis shown in the previous sections represent some preliminary steps toward objectively finding and comparing aspects of TC structure. While it is not feasible to catalogue all convective scale features, this basic climatology of inner-core signals allows the internal evolution of the TC to be considered and related to different storms. Based on both the case study and compositing of thousands of satellite overpasses, it appears there is utility in cataloguing structural markers of TCs to differentiate between intensity and structure regimes. These structural traits can further be used to discern patterns of TC life-cycle evolution, with potential applications towards diagnosing and forecasting intensity.

7. ACKNOWLEDGEMENTS

The authors greatly appreciate Ken Knapp and his team for the HURSAT dataset and feedback. Constructive discussion has also been provided by Jeff Hawkins and Chris Velden, who with Tony Wimmers have been instrumental by providing their ARCHER technique. This research has been supported by NASA GRIP Grant #NNX09AC43G, an AMS (SAIC) graduate fellowship, and an FSU presidential fellowship.

8. REFERENCES

Burpee, R. W., J. L. Franklin, S. J. Lord, R. E. Tuleya, and S. D. Aberson, 1996: The impact of Omega dropwindsondes on operational hurricane track forecast models. *Bull. Amer. Meteor. Soc.*, **77**, 925–933.

Cangialosi, J. P. and J. L. Franklin, 2012: 2011 National Hurricane Center Forecast Verification Report. National Hurricane Center. NOAA/NWS/NCEP/Tropical Prediction Center.

DeMaria, Mark, Michelle Mainelli, Lynn K. Shay, John A. Knaff, John Kaplan, 2005: Further Improvements to the Statistical Hurricane Intensity Prediction Scheme (SHIPS). *Wea. Forecasting*, **20**, 531–543.

Dvorak, V. F., 1975: Tropical cyclone intensity analysis and forecasting from satellite imagery. *Mon. Wea. Rev.*, **103,** 420–430.

Knapp, K. R., 2008: Hurricane satellite (HURSAT) data sets: Low-earth orbit infrared and microwave data. Preprints, *28th Conf. on Hurricanes and Tropical Meteorology*, Orlando, FL, Amer. Meteor. Soc., 4B.4.

Hawkins, Jeffrey D., Thomas F. Lee, Joseph Turk, Charles Sampson, John Kent, Kim Richardson, 2001: Real–Time Internet Distribution of Satellite Products for Tropical Cyclone Reconnaissance. *Bull. Amer. Meteor. Soc.*, **82**, 567–578.

Murray, D.A., 2009: Improved Short-Term Atlantic Hurricane Intensity Forecasts Using Reconnaissance-based Core Measurements. M.S. Thesis, Florida State University, 150 pp.

Olander, T., and C. Velden, 2007: The advanced Dvorak technique: Continued development of an objective scheme to estimate tropical cyclone intensity using geostationary infrared satellite imagery. *Wea. Forecasting*, **22,** 287–298.

Piech, D., 2007: Atlantic Reconnaissance Vortex Message Climatology and Composites and Their Use in Characterizing Eyewall Cycles. M.S. Thesis, Florida State University, 139 pp.

Sampson, Charles R., James L. Franklin, John A. Knaff, Mark DeMaria, 2008: Experiments with a Simple Tropical Cyclone Intensity Consensus. *Wea. Forecasting*, **23**, 304–312.

Wang, Y., and C-C. Wu, 2004: Current understanding of tropical cyclone structure and intensity changes—A review. *Meteor. Atmos. Phys.*, **87,** 257–278.

Wimmers, Anthony J., and Christopher S. Velden, 2010: Objectively Determining the Rotational Center of Tropical Cyclones in Passive Microwave Satellite Imagery. *J. Appl. Meteor. Climatol.*, **49**, 2013–2034.